Eco-Driving of Autonomous Vehicles for Nonstop Crossing of Signalized Intersections

Xiangyu Meng and Christos G. Cassandras, *Life Fellow, IEEE*

***Abstract*— This article is devoted to the development of an optimal speed profile for autonomous vehicles in order to cross a signalized intersection without stopping. The design objective is to achieve both a short travel time and low energy consumption by taking full advantage of the traffic light information based on vehicle-to-infrastructure communication. The eco-driving problem is formulated as an optimal control problem. For the case where the vehicles are in free-flow mode, we derive a real-time on-line analytical solution, distinguishing our method from most existing approaches based on numerical calculations. Under mild assumptions, the optimal eco-driving algorithm is readily extended to cases where the free-flow mode does not apply due to the presence of interfering traffic. Extensive simulations are provided to compare the performance of autonomous vehicles under the proposed speed profile and human-driven vehicles. The results show quantitatively the advantages of the proposed algorithm in terms of energy consumption and travel time.**

***Note to Practitioners*—This article is motivated by the requirements for increased safety, increased efficiency in energy consumption, and lower congestion in signalized intersections. We take advantage of the traffic signal phase and timing information based on vehicle to infrastructure communication, and use the information to plan the vehicle's trajectory to avoid the red traffic signal. An optimal speed profile is developed to achieve a trade-off between minimizing trip time and avoiding unnecessary braking and acceleration which corresponds to minimizing energy consumption. We then show how such a speed profile can be efficiently computed and control the motion of an autonomous vehicle (or serve as an intelligent speed advisory system for human-driven vehicles) leading to a safe, time-efficient, and energy-efficient trip. A video of a real autonomous vehicle test implementing our control algorithm can be found at https://www.youtube.com/watch?v=x-ao4szeLYo.**

Manuscript received February 8, 2020; revised May 26, 2020 and August 8, 2020; accepted September 28, 2020. This article was recommended for publication by Associate Editor V. Stojanovic and Editor Q. Zhao upon evaluation of the reviewers' comments. This work was supported in part by NSF under Grant ECCS-1509084, Grant DMS-1664644, and Grant CNS-1645681; in part by AFOSR under Grant FA9550-19-1-0158; in part by the ARPA-E's NEXTCAR Program under Grant DE-AR0000796; and in part by MathWorks. *(Corresponding author: Xiangyu Meng.)*

Xiangyu Meng is with the Division of Electrical and Computer Engineering, Louisiana State University, Baton Rouge, LA 70803 USA (e-mail: xmeng5@lsu.edu).

Christos G. Cassandras is with the Division of Systems Engineering, Center for Information and Systems Engineering, Boston University, Brookline, MA 02446 USA (e-mail: cgc@bu.edu).

This article has supplementary downloadable material available at http://ieeexplore.ieee.org, provided by the authors.

Color versions of one or more of the figures in this article are available online at http://ieeexplore.ieee.org.

Digital Object Identifier 10.1109/TASE.2020.3029452

***Index Terms*— Autonomous vehicles, eco-driving, input constraint, optimal control, state constraint, vehicle-to-infrastructure (V2I) communication.**

I. Introduction

THE alarming state of existing transportation systems has been well documented. For instance, in 2014, congestion caused vehicles in urban areas to spend 6.9 billion additional hours on the road at a cost of an extra 3.1 billion gallons of fuel, resulting in a total cost estimated at $160 billion [1]. From a control and optimization standpoint, the challenges stem from requirements for increased safety, increased efficiency in energy consumption, and lower congestion both in highway and urban traffic. Connected and automated vehicles (CAVs) provide an intriguing opportunity for enabling users to better monitor transportation network conditions and to improve traffic flow [2]. Their proliferation has rapidly grown, largely as a result of vehicle-to-X (or V2X) technology [3] which refers to an intelligent transportation system where all vehicles and infrastructure components are interconnected with each other. Such connectivity provides precise knowledge of the traffic situation across the entire road network, which in turn helps optimize traffic flows, enhance safety, reduce congestion, and minimize emissions. Controlling a vehicle to improve energy consumption has been studied extensively [4], [5]. In general, there are two types of intersections including signalized and unsignalized intersections. In signalized intersections, green and red cycle lengths can be dynamically controlled [6]. For unsignalized intersections, work in this area focuses on coordinating vehicles [7]–[9]. More recently, an optimal control framework is proposed in [10] for CAVs to cross one or two adjacent intersections in an urban area. The state-of-the-art and current trends in the coordination of CAVs are provided in [11].

Our focus in this article is on an optimal control approach for a single autonomous vehicle approaching a signalized intersection in an energy-efficient way by exploiting traffic signal information available through vehicle-to-infrastructure (V2I) communication. An optimal control problem (OCP) solution provides a lower performance bound so we know what the "best" we can achieve is. This solution provides: 1) a "reference" to track during real-time execution using on-line methods like model predictive control (MPC) [12] or the control barrier function (CBF) approach as in [13] and 2) a way to quantify how any such method (or any other "practical" method) performs relative to the OCP lower

bound. Compared with the preliminary version of the free-flow model studied in [14], in this article we provide a complete technical treatment that includes both the free-flow mode with proofs of all theorems and its extension to interfering traffic, as well as extensive simulations to illustrate the analysis, a quantification of the eco-driving benefits through a detailed energy consumption model, and a comparison with a human-driving behavior model in VISSIM. The term "ECO-AND" (short for "Economical Arrival and Departure") is often used in the literature to refer to this problem [15]. Its solution is made possible by V2I communication, which enables a vehicle to automatically receive signals from upcoming traffic lights before they appear in its visual range. For example, such a V2I communication system has been launched in Audi cars at more than 4700 intersections across the United States by offering a traffic light timer on their dashboards: as the car approaches an intersection, a red traffic signal symbol and a "time-to-go" countdown appear in the digital display and reads how long it will be before the traffic signal ahead turns green. Clearly, an autonomous vehicle can take advantage of such information in order to go beyond current "stop-and-go" to achieve "stop-free" driving. Along these lines, the problem of avoiding red traffic signals at a single intersection is investigated in [16]–[20]. The purpose in [16] is to track a target speed profile, which is generated based on the feasibility of avoiding a sequence of red lights. The MPC approach was used based on a receding horizon. The work in [18] devises the optimal speed profile given the feasible target time, which is within some green light interval. GlidePath system proposed in [19] is equipped with a scenario identifier component, and target velocity is provided for each scenario. Dynamic programming is employed in [20] to solve the eco-driving control problem with unknown traffic light signal timing. The case of multiple signalized intersections is considered in [21]–[24]. Avoiding red lights with probabilistic information at multiple intersections was considered in [21], where the time horizon is discretized and deterministic dynamic programming is utilized to numerically compute the optimal control input. A velocity pruning algorithm is proposed in [22] to identify feasible green windows, and a velocity profile is calculated numerically in terms of energy consumption. Minimizing the fuel consumption between two red-signalized intersections is considered in [23], where the Legendre pseudospectral algorithm is used to numerically solve the problem. The optimality analysis in [24] was first used to identify the structure of the optimal acceleration profile, which is then characterized by several parameters. The parameters are optimized to seek the best performance. The results in [24] show that the performance is significantly improved by using the information of multiple signalized intersections together.

In this article, an optimal control approach is used to design an optimal speed profile for autonomous vehicles approaching a signalized intersection. The optimality of the speed profile is in the sense that it minimizes an objective function of a weighted sum of both trip time and energy cost. Several factors, such as the nonconvexity of the feasible green signal interval, and the state constraints related to speed limits and a safe following distance, make the problem difficult to solve. To overcome these difficulties, we first devise a free flow solution and then extend it to the non-free flow case. For the free flow mode, we first derive a solution without taking into account the traffic signal constraint, that is, the discontinuous interval constraints are removed. If the terminal time obtained from the above solution falls within some green signal interval, then the traffic signal constraint is satisfied automatically. When, instead, the terminal time falls within some red signal interval, then the feasible terminal time could be either the end of the previous green signal interval or the beginning of the next green signal interval. Then, we transform the original problem into a fixed terminal time OCP, which is solved with two feasible terminal times. Comparing the corresponding performances leads to the optimal solution of the free flow case. We also show that the optimal eco-driving algorithm derived under free flow conditions can be adjusted to handle the case with interfering traffic under the assumption that some traffic information is available. Kamal *et al.* [25] studied an energy-efficient driving strategy on roads with varying traffic signals at intersections with the goal of following the host vehicle driven by a human instead of avoiding red traffic signals.

The main contributions of this article are as follows.

1) Instead of solving this problem numerically as in some of the existing work, an explicit analytical solution is obtained.
2) We jointly optimize the energy consumption and the throughput, unlike existing work which optimizes one of them or optimizes both separately. We also explore the tradeoff between the energy consumption and the throughput.
3) Due to the on-line and real-time nature of the algorithm, the speed profile can be recalculated as needed or can be adjusted to consider interfering traffic from other road users.

The remainder of this article is organized as follows. The problem is formulated in Section II. In Section III, we present the methodology to solve the formulated problem, where the solution to the free terminal time OCP is described in Section III-A, and the solution to the fixed terminal time OCP is presented in Section III-B. Section IV shows how the optimal solution can be extended to include the case when execution of the optimal trajectory is obstructed by other road users. Simulation results illustrating the use of the proposed algorithm are presented in Section V. Section VI summarizes our findings, concludes this article, and provides directions for future work.

II. Problem Formulation

In order to produce reliable results for eco-driving problems, it is crucial to include powertrain dynamics of a vehicle in design optimization. However, due to the complexity of powertrain dynamics, it is impractical to do so in scenarios which require real-time calculations. Therefore, we adopt a two-level approach, where the high level is to provide a real-time reference speed profile for the powertrain dynamics based on a purely kinematic model (1), and we assume

that in the low level proportional-integral-derivative (PID) controllers or model predictive controllers are available to the vehicle powertrain dynamics for reference speed tracking. The dynamics of the vehicle are modeled by a double integrator

$$\dot{x}(t) = v(t), \qquad \dot{v}(t) = u(t) \tag{1}$$

where $x(t)$, $v(t)$, and $u(t)$ are the position, velocity, and acceleration of the vehicle, respectively. At time t_0, the initial position and velocity are given as $x(t_0) = 0$ and $v(t_0) = v_0$, respectively. The acceleration term $u(t)$ includes an air resistance term $-v^2(t)$, which is not explicitly shown in (1). The inclusion of $-v^2(t)$ explicitly in $u(t)$ will complicate the analysis and hinder us from obtaining real-time solutions. On the road, there are other users which may affect the movement of the autonomous vehicle. Therefore, we consider the interference of the preceding human-driven vehicles whose trajectory is given by $x_p(t)$. The distance between the preceding human-driven vehicle and the autonomous vehicle is defined as $d(t) = x_p(t) - x(t)$. Let us use l to denote the distance to the traffic light, and t_p the intersection crossing time of the vehicle. The traffic signals switch between green and red at an intersection, where the set of green intervals is T_G, and the set of red intervals is T_R.

Our objective is to make the vehicle cross an intersection without stopping with the aid of traffic signal information as well as to minimize both travel time and energy consumption. Thus, we formulate the following problem:

Problem 1: ECO-AND Problem

$$\min_{u(t),t_p} \quad \rho_t(t_p - t_0) + \rho_u \int_{t_0}^{t_p} u^2(t)dt \tag{2}$$

$$\text{s. t. (1)}, \ x(t_p) = l \tag{3}$$

$$v_{\min} \le v(t) \le v_{\max} \tag{4}$$

$$u_{\min} \le u(t) \le u_{\max} \tag{5}$$

$$d(t) \ge \alpha v(t) + \beta \tag{6}$$

and

$$t_p \in T_G \tag{7}$$

where $\beta > 0$ relates to a static safety distance, that is, the distance when both vehicles stop and $\alpha > 0$ relates to a dynamic braking distance [26]. In (2), the term $J^t = t_p - t_0$ is the travel time while $J^u = \int_{t_0}^{t_p} u^2(t)dt$ penalizes acceleration which indirectly helps energy saving and passenger riding comfort [27]. There are also results in the literature showing that pulse and glide operation of a combustion engine may reduce fuel consumption at low speeds [28]. The parameters $v_{\min} > 0$ and $v_{\max} > 0$ are the minimum and maximum allowable speeds for road vehicles, respectively, while the parameters $u_{\min}$ and $u_{\max}$ are the maximum allowable deceleration and acceleration, respectively.

In order to normalize these two terms for the purpose of a well-defined optimization problem, first note that the maximum possible value of J^t is $l/v_{\min}$. Depending on the relationship between $v_{\min}$, $v_{\max}$, $u_{\max}$ and l, there are two different cases for the maximum possible value of J^u. The first case is when the road length is long enough so that the vehicle can accelerate from $v_{\min}$ to $v_{\max}$ by using the maximum acceleration $u_{\max}$, i.e., when $l \ge v_{\min}(v_{\max} - v_{\min})/u_{\max} + (v_{\max} - v_{\min})^2/(2u_{\max})$. In this case,

$$J^u = \frac{v_{\max} - v_{\min}}{u_{\max}} u_{\max}^2 = (v_{\max} - v_{\min})u_{\max}.$$

The second case is when the road length is not long enough for the vehicle to accelerate to the maximum speed. According to the dynamics (1), we have $v_{\min}(t_p - t_0) + u_{\max}(t_p - t_0)^2/2 = l$. By solving the above quadratic equation, we are able to get

$$t_p - t_0 = \frac{\sqrt{v_{\min}^2 + 2u_{\max}l} - v_{\min}}{u_{\max}}.$$

Therefore, in this case,

$$J^u = \int_{t_0}^{t_p} u_{\max}^2 dt = \left(\sqrt{v_{\min}^2 + 2u_{\max}l} - v_{\min}\right)u_{\max}.$$

We can now specify the two weighting parameters ρ_t and ρ_u as follows: $\rho_t = \rho v_{\min}/l$ and

$$\rho_u = \begin{cases} \dfrac{1-\rho}{(v_{\max} - v_{\min})u_{\max}}, & \text{if } \ l \ge v_{\min}\dfrac{v_{\max} - v_{\min}}{u_{\max}} \\ & \quad + \dfrac{1}{2}\dfrac{(v_{\max} - v_{\min})^2}{u_{\max}} \\ \dfrac{1-\rho}{(\sqrt{v_{\min}^2 + 2u_{\max}l} - v_{\min})u_{\max}}, & \text{otherwise} \end{cases}$$

capturing the normalized tradeoff between the travel time and energy consumption by setting $0 \le \rho \le 1$. When $\rho = 0$, the problem reduces to minimizing the energy consumption only; when $\rho = 1$, we seek to minimize the travel time only.

Note that when $u < 0$, the vehicle decelerates due to braking and when $u > 0$ the vehicle accelerates. Finally, the constraint (7) reflects the requirement that t_p belongs to an interval when the traffic signal is green.

III. Main Results

The challenges of the ECO-AND problem stem from the constraints (6) and (7). To ensure the satisfaction of (6), an accurate prediction of the road traffic conditions and the driving behavior of the preceding vehicle is needed. We first relax (6), i.e., we consider cases where the vehicle is in free-flow mode, and show how the result without considering (6) can be extended to include (6) based on mild assumptions in Section IV.

The constraint (7) is a disconnected set constraint, which makes the problem nonconvex. Existing approaches to such problems turn out to be very demanding for off-line computation, not to mention obtaining analytical solutions in a real-time on-line context. We proceed by relaxing the constraint (7) as well, which allows us to efficiently obtain an analytical solution on-line. If the optimal arrival time t_p^* is within some green interval, then the free-flow problem is solved. However, if $t_p^* \in T_R$, then we solve Problem 1 twice but with constraint (7) replaced by $t_p = \underline{t}_p = \sup\{t < t_p^* | t \in T_G\}$, and $t_p = \bar{t}_p = \inf\{t > t_p^* | t \in T_G\}$, respectively. In simple terms, if the optimal terminal time of the problem without (7) does

not allow the vehicle to make the green light, then we compare the performance obtained with different terminal times, and the solution produced by the one with better performance is the most likely optimal solution. To confirm this, we can plot the optimal performance $J^*(t_p)$ as a function of the terminal time t_p to explicitly determine the optimal terminal time t_p^*.

Let us first introduce a lemma, which will be used frequently throughout the following analysis.

Lemma 1: Consider the vehicle dynamics (1) with the initial conditions x_0 and v_0. If the control input $u(t) = a$ is constant during the time interval $[t_0, t_1]$, then

$$\begin{aligned} v(t_1) &= v_0 + a(t_1 - t_0) \\ x(t_1) &= x_0 + v_0(t_1 - t_0) + \frac{1}{2}a(t_1 - t_0)^2 \\ J^u &= a^2(t_1 - t_0). \end{aligned}$$

If the control input $u(t) = a(t_1 - t)$ with a constant a, then

$$\begin{aligned} v(t_1) &= v_0 + \frac{1}{2}a(t_1 - t_0)^2 \\ x(t_1) &= x_0 + v_0(t_1 - t_0) + \frac{1}{3}a(t_1 - t_0)^3 \\ J^u &= \frac{1}{3}a^2(t_1 - t_0)^3. \end{aligned}$$

Proof: The proof is given in [29]. ∎

In the following, we first seek the optimal solution to Problem 1 without the constraint (7), which is termed "free terminal time OCP."

A. Free Terminal Time Optimal Control Problem

The free terminal time OCP is given in the following.

Problem 2: Free terminal time OCP

$$\min_{u(t), t_p} \rho_t(t_p - t_0) + \rho_u \int_{t_0}^{t_p} u^2(t)dt \tag{8}$$

$$\text{s. t. (1)}, \quad x(t_p) = l \tag{9}$$

$$v_{\min} \le v(t) \le v_{\max} \tag{10}$$

$$u_{\min} \le u(t) \le u_{\max} \tag{11}$$

where ρ_t and ρ_u are given in Section II.

For the objective function (8), we prove that the optimal solution is to never decelerate, that is, $u(t) \ge 0$ for $t \in [t_0, t_p]$, which is shown in Lemma 2.

Lemma 2: The optimal solution $u^*(t)$ to Problem 2 satisfies $u^*(t) \ge 0$ for all $t \in [t_0, t_p^*]$.

Proof: The proof is given in [29]. ∎

In addition, we have the following result for the optimal acceleration profile.

Lemma 3: In the optimal acceleration profile, acceleration always precedes cruising at constant speed.

Proof: The proof is given in [29]. ∎

Whenever $v(\tau) = v_{\max}$ for some $\tau \in [t_0, t_p]$ (which may not be possible in some cases), we must have $u(t) = 0$ for all $t \in [\tau, t_p]$. Based on these properties of the optimal solution, we can derive necessary conditions for the solution to Problem 2, which are summarized in Theorem 1.

Theorem 1: Consider the vehicle's dynamics (1) with initial conditions $x(t_0) = 0$ and $v(t_0) = v_0$. Let $x^*(t)$, $v^*(t)$, $u^*(t)$, t_p^* be an optimal solution to Problem 2 and assume that $\rho_t \neq 0$ and $\rho_u \neq 0$. Then, the optimal control $u^*(t)$ satisfies

$$u^*(t) = \arg \min_{0 \le u(t) \le u_{\max}} \rho_u u^2(t) + \frac{\rho_t}{v^*(t_p^*)}(t - \tau)u(t) \tag{12}$$

where τ is the first time on the optimal path when $v(\tau) = v_{\max}$ if $\tau < t_p$; $\tau = t_p^*$ otherwise.

Proof: Here, we use the direct adjoining approach in [30] to obtain necessary conditions for the optimal solution $u^*(t)$ and t_p^*, where $*$ denotes optimal quantities. The Hamiltonian $H(v, u, \lambda)$ and Lagrangian $L(v, u, \lambda, \mu, \eta)$ are defined as

$$H(v, u, \lambda) = \rho_u u^2 + \rho_t + \lambda_1 v + \lambda_2 u \tag{13}$$

and

$$\begin{aligned} L(v, u, \lambda, \mu, \eta) = H(v, u, \lambda) + \mu(u - u_{\max}) \\ + \eta_1(v_{\min} - v) + \eta_2(v - v_{\max}) \end{aligned} \tag{14}$$

respectively, where $\lambda(t) = [\lambda_1(t)\ \lambda_2(t)]^T$ and $\eta(t) = [\eta_1(t)\ \eta_2(t)]^T$

$$\mu(t) \ge 0, \quad \mu(t)[u^*(t) - u_{\max}] = 0 \tag{15}$$

$$\eta_1(t) \ge 0, \quad \eta_2(t) \ge 0$$

$$\eta_1(t)[v_{\min} - v^*(t)] + \eta_2(t)[v^*(t) - v_{\max}] = 0. \tag{16}$$

Note that we did not include the constraint $u(t) \ge u_{\min}$ since we have already established that the optimal control satisfies $u^*(t) \ge 0$ in the free terminal time OCP in Lemma 2. According to Pontryagin's minimum principle, the optimal control $u^*(t)$ must satisfy

$$u^*(t) = \arg \min_{0 \le u(t) \le u_{\max}} H(v^*(t), u(t), \lambda(t)) \tag{17}$$

which allows us to express $u^*(t)$ in terms of the costate $\lambda(t)$, resulting in

$$u^*(t) = \min\left\{u_{\max}, -\frac{\lambda_2(t)}{2\rho_u}\right\} \tag{18}$$

with $\lambda_2(t) \le 0$ due to Lemma 2. The Lagrange multiplier $\mu(t)$ is such that

$$\frac{\partial L^*}{\partial u}|_{u=u^*(t)} = 2\rho_u u^*(t) + \lambda_2(t) + \mu(t) = 0. \tag{19}$$

Since we can always find $\mu(t) \ge 0$ to make (15) and (19) hold under the minimum principle (15), (18), and (19) can be considered as redundant conditions. For the costate $\lambda_1(t)$, we have $\dot{\lambda}_1(t) = -\partial L^*(t)/\partial x = 0$, which means $\lambda_1(t) = \lambda_1$ is a constant. The costate $\lambda_2(t)$ satisfies

$$\dot{\lambda}_2(t) = -\frac{\partial L^*(t)}{\partial v} = -\lambda_1 + \eta_1(t) - \eta_2(t). \tag{20}$$

First, let us use a proof by contradiction to show that if $v^*(t) = v_{\min}$, then $t = t_0$. Assume that there exists a t such that $v^*(t) = v_{\min}$. Then, we must have $v^*(t) = v_{\min}$ for all $t \in [t_0, t_p^*]$ due to Lemma 3. According to the system dynamics in (1), $u(t) = 0$ for all $t \in [t_0, t_p^*]$. Based on the minimum principle (18), $\lambda_2(t) = 0$ for all $t \in [t_0, t_p^*]$. From (16), we know that $\eta_2(t) = 0$ for all $t \in [t_0, t_p^*]$. Since the terminal time t_p is unspecified, there is a necessary transversality condition for t_p^* to be optimal, namely, $H(v^*(t_p^*), u^*(t_p^*), \lambda(t_p^*)) = 0$, that is

$$\rho_u u^*\left(t_p^*\right)^2 + \rho_t + \lambda_1 v^*\left(t_p^*\right) + \lambda_2\left(t_p^*\right)u\left(t_p^*\right) = 0. \tag{21}$$

Since $u^*(t_p^*) = 0$, we must have $\lambda_1 < 0$ according to (21). Then, we obtain $\dot{\lambda}_2(t) > 0$ from (20), which contradicts $\lambda_2(t) = 0$ for $t \in [t_0, t_p^*]$. We have thus established that if $v^*(t) = v_{\min}$, then $t = t_0$. Next, we will show that $\lambda_2(t)$ has no discontinuities. Since it is impossible that $v(t) = v_{\min}$ for $t \neq t_0$, the costate trajectory $\lambda_2(t)$ may jump only at some time τ when $v(\tau) = v_{\max}$. When the state constraint does not depend on t explicitly, we have the condition [31] $H^*(\tau^-) = H^*(\tau^+)$, which can be written as

$$\rho_u u^*(\tau^-)^2 + \lambda_2(\tau^-)u^*(\tau^-) = \rho_u u^*(\tau^+)^2 + \lambda_2(\tau^+)u^*(\tau^+) \tag{22}$$

where τ^+ and τ^- denote the left-hand side and the right-hand side limits, respectively. We know from Lemma 2 that $u^*(t) = 0$, for $t \in [\tau, t_p^*]$. Therefore, from (22), we obtain

$$\rho_u u^*(\tau^-)^2 + \lambda_2(\tau^-)u^*(\tau^-) = 0. \tag{23}$$

According to (18), we either have $u^*(\tau^-) = -\lambda_2(\tau^-)/(2\rho_u)$ or $u^*(\tau^-) = u_{\max}$. When $u^*(\tau^-) = -\lambda_2(\tau^-)/(2\rho_u)$, (23) becomes $-\rho_u u^*(\tau^-)^2 = 0$, which implies $u^*(\tau^-) = \lambda_2(\tau^-) = 0$. When $u^*(\tau^-) = u_{\max}$, (23) becomes $u_{\max} = -\lambda_2(\tau^-)/\rho_u$, which contradicts condition (18) where $u_{\max} \leq -\lambda_2(\tau^-)/(2\rho_u)$. Therefore, only the case $u^*(\tau^-) = \lambda_2(\tau^-) = 0$ is possible. In other words, the costate trajectory $\lambda_2(t)$ has no discontinuities, and the following jump conditions:

$$\lambda_2(\tau^-) = \lambda_2(\tau^+) - \zeta_1(\tau) + \zeta_2(\tau) \tag{24}$$

$\zeta_1(\tau) \geq 0$, $\zeta_2(\tau) \geq 0$, and

$$\zeta_1(\tau)[v_{\min} - v^*(\tau)] + \zeta_2(\tau)[v^*(\tau) - v_{\max}] = 0 \tag{25}$$

are always satisfied with $\zeta_1(\tau) = \zeta_2(\tau) = 0$. Next, we will show that $\lambda_2(t_p^*) = 0$. At the terminal time t_p^*, the following transversality conditions hold [30]:

$$\lambda_2\left(t_p^{*-}\right) = \gamma_1 \frac{\partial}{\partial v}[v_{\min} - v]|_{v=v^*(t_p^*)} + \gamma_2 \frac{\partial}{\partial v}[v - v_{\max}]\big|_{v=v^*\left(t_p^*\right)}$$

that is, $\lambda_2(t_p^{*-}) = -\gamma_1 + \gamma_2$ where $\gamma_1 \geq 0$, $\gamma_2 \geq 0$, and

$$\gamma_1\left[v_{\min} - v^*\left(t_p^*\right)\right] + \gamma_2\left[v^*\left(t_p^*\right) - v_{\max}\right] = 0. \tag{26}$$

If $v_{\min} < v^*(t_p^*) < v_{\max}$, then $\gamma_1 = \gamma_2 = 0$, which leads to $\lambda_2(t_p^*) = 0$ by the continuity of $\lambda_2(t)$. When $v^*(t_p^*) = v_{\max}$, then $u^*(t_p^*) = 0$, which results in $\lambda_2(t_p^*) = 0$ according to (18). Last, we will show that $\eta_1(t) = 0$, and

$$\eta_2(t) = \begin{cases} 0, & \text{for } t \in [t_0, \tau) \\ -\lambda_1, & \text{for } t \in [\tau, t_p^*]. \end{cases}$$

Since $H(v, u, \lambda)$ is not an explicit function of time t, it follows that $dH^*(t)/dt = 0$, that is

$$[2\rho_u u^*(t) + \lambda_2(t)]\dot{u}^*(t) + [\eta_1(t) - \eta_2(t)]u^*(t) = 0. \tag{27}$$

The first term $[2\rho_u u^*(t) + \lambda_2(t)]\dot{u}^*(t)$ is always zero since when $u^*(t) \neq u_{\max}$, $2\rho_u u^*(t) + \lambda_2^*(t) = 0$ according to (18), and when $u^*(t) = u_{\max}$, $\dot{u}^*(t) = 0$. Condition (27) can thus be reduced to

$$[\eta_1(t) - \eta_2(t)]u^*(t) = 0. \tag{28}$$

When $v_0 = v_{\min}$, we have $\eta_2(t_0) = 0$ from the fact that if $v^*(t) = v_{\min}$, then $t = t_0$ shown earlier and from (16). Condition (28) then implies $\eta_1(t_0)u^*(t_0) = 0$. Since $u^*(t_0) > 0$ according to Lemma 3, we can get $\eta_1(t_0) = 0$. Then $\eta_1(t) = 0$ since $v(t) > v_{\min}$ for $t > t_0$. Therefore, for any v_0, we have $\eta_1(t) = 0$. It is easy to get from (16) that $\eta_2(t) = 0$ for $t \in [t_0, \tau)$. For $t \in [\tau, t_p^*]$, $\eta_2(t) = -\lambda_1$ satisfies condition (16) and $\dot{\lambda}_2(t) = 0$ in (20). Based on the above observations, the differential equation (20) becomes

$$\dot{\lambda}_2(t) = -\lambda_1 \tag{29}$$

for $t \in [t_0, \tau)$. Because of (18) and $\lambda_2(t_p^*) = 0$ (shown earlier), we have $u^*(t_p^*) = 0$, and then $-\lambda_1 = \rho_t / v^*(t_p^*)$ from (21). Solving the differential equation (29), we have

$$\lambda_2(t) = \frac{\rho_t}{v^*\left(t_p^*\right)}(t - \tau) \tag{30}$$

for $t \in [t_0\, \tau]$. In the case that $v^*(t_p^*) < v_{\max}$, we simply let $\tau = t_p^*$ in (30). The proof is completed by substituting (30) for $\lambda_2(t)$ in (17). ■

Recall that the theorem was proved under the assumption that $\rho_t \neq 0$ and $\rho_u \neq 0$. The special cases when either $\rho_t = 0$ or $\rho_u = 0$ are considered in Corollaries 2 and 3.

Corollary 2: Consider the vehicle dynamics (1) with initial conditions $x(t_0) = 0$ and $v(t_0) = v_0$. Let $x^*(t)$, $v^*(t)$, $u^*(t)$, t_p^* be an optimal solution to Problem 2 when $\rho_t = 0$. Then, the optimal control $u^*(t)$ satisfies $u^*(t) = 0$ for all $t \in [t_0, t_p^*]$.

Corollary 3: Consider the vehicle dynamics (1) with initial conditions $x(t_0) = 0$ and $v(t_0) = v_0$. Let $x^*(t)$, $v^*(t)$, $u^*(t)$, t_p^* be an optimal solution to Problem 2 when $\rho_u = 0$. Then, the optimal control $u^*(t)$ satisfies

$$u^*(t) = \begin{cases} u_{\max}, & \text{for } t \in [t_0, \tau) \\ 0, & \text{for } t \in \left[\tau, t_p^*\right] \end{cases} \tag{31}$$

where τ is the first time on the optimal path when $v^*(\tau) = v_{\max}$.

The proofs of the above two corollaries are straightforward by setting $\rho_t = 0$ and $\rho_u = 0$, respectively, in (12) in Theorem 1.

Based on the vehicle dynamics (1), the initial conditions $x(t_0) = 0$ and $v(t_0) = v_0$, and the terminal condition $x^*(t_p^*) = l$, the optimal control law (12) and the optimal time t_p^* can be uniquely determined. In the following, we will classify the results into different cases depending on the values of the model parameters. In order to do so, we define two functions

$$f(v_0) = l - \frac{v_{\max}^2 - v_0^2}{2u_{\max}} - u_{\max} v_{\max}^2 \frac{\rho_u}{\rho_t} + \frac{1}{6} u_{\max}^3 v_{\max}^2 \frac{\rho_u^2}{\rho_t^2}$$

$$g(v_0) = l - 2v_0\sqrt{(v_{\max} - v_0)v_{\max}\frac{\rho_u}{\rho_t}} - \frac{4}{3}(v_{\max} - v_0)\sqrt{(v_{\max} - v_0)v_{\max}\frac{\rho_u}{\rho_t}}.$$

Depending on the signs of these two functions, the optimal solution consisting of $u^*(t)$ and t_p^* can be classified as shown in Table I with all detailed calculations provided in [29].

TABLE I
OPTIMAL SOLUTION CLASSIFICATION FOR PROBLEM 2

	$\frac{v_0}{v_{\max}} < 1 - u_{\max}^2 \frac{\rho_u}{\rho_t}$		$1 - u_{\max}^2 \frac{\rho_u}{\rho_t} \leq \frac{v_0}{v_{\max}}$	
	$f(v_0) \geq 0$	$f(v_0) < 0$	$g(v_0) \geq 0$	$g(v_0) < 0$
u^*	$\Phi\left(t \mid t_1, t_2, \frac{\rho_t}{2\rho_u v_{\max}}\right)$	$\Phi\left(t \mid t_3, -, \frac{\rho_t}{2\rho_u v_1}\right)$	$\Phi\left(t \mid -, t_4, \frac{\rho_t}{2\rho_u v_{\max}}\right)$	$\Phi\left(t \mid -, -, \frac{\rho_t}{2\rho_u v_2}\right)$
t_p^*	δ_1	δ_2	δ_3	δ_4

Referring to this table, the optimal control is parameterized by the following function:

$$\Phi(t|a,b,c) = \begin{cases} u_{\max}, & \text{when } t \leq a \\ c(t-b), & \text{when } a < t < b \\ 0, & \text{when } t \geq b \end{cases} \tag{32}$$

where the dash $(-)$ in Φ in Table I means that the variable t is not defined on the corresponding domain, and therefore that case is inapplicable here. The parameters shown in Table I are defined as follows:

$$t_1 = t_0 + \frac{(1 - u_{\max}^2 \frac{\rho_u}{\rho_t}) v_{\max} - v_0}{u_{\max}}, \; t_3 = t_0 + \frac{v_1 - v_0}{u_{\max}}$$

$$t_2 = t_1 + 2u_{\max} v_{\max} \frac{\rho_u}{\rho_t}, \; t_4 = t_0 + 2\sqrt{(v_{\max} - v_0) v_{\max} \frac{\rho_u}{\rho_t}}$$

where

$$v_1 = \sqrt{\frac{2u_{\max} l + v_0^2}{1 + \frac{4u_{\max}^2}{1 - \frac{\rho_u}{\rho_t} u_{\max}^2} \frac{\rho_u}{\rho_t} + \frac{8}{3} \frac{u_{\max}^4}{(1 - \frac{\rho_u}{\rho_t} u_{\max}^2)^2} \frac{\rho_u^2}{\rho_t^2}}}$$

and v_2 is the solution of the following equation:

$$l = \frac{2}{3}(v_0 + 2v_2)\sqrt{(v_2 - v_0) v_2 \frac{\rho_u}{\rho_t}}.$$

The parameters $\delta_1, \delta_2, \delta_3, \delta_4$ in Table I specifying the optimal time t_p^* when the vehicle arrives at the intersection in each of the four possible cases are given in the following:

$$\delta_1 = t_2 + \frac{f(v_0)}{v_{\max}}, \quad \delta_2 = t_3 + 2u_{\max} \frac{v_1}{1 - \frac{\rho_u}{\rho_t} u_{\max}^2} \frac{\rho_u}{\rho_t}$$

$$\delta_3 = t_4 + \frac{g(v_0)}{v_{\max}}, \quad \delta_4 = t_0 + 2\sqrt{(v_2 - v_0) v_2 \frac{\rho_u}{\rho_t}}.$$

Remark 1: This remark pertains to the underlying criteria for the optimal solution classification in Table I. The first row determines whether or not the maximum acceleration $u_{\max}$ will be used for a given initial speed v_0. The optimality conditions tell us that the vehicle starts with the maximum acceleration when the initial speed is relatively low, which corresponds to a positive value of a in Φ in (32). The second row determines if the road length l is large enough for a vehicle to reach its maximum speed for a given initial speed v_0. In general, the optimal control contains three phases: full acceleration, linearly decreasing acceleration, and no acceleration, which is defined by Φ in (32). The first column specifies the case where all three phases are included with switches defined by t_1, t_2. The second column corresponds to the case of low initial speeds and short-length roads. Under optimal control in this case, the vehicle starts with full acceleration, but the road length is so short that the maximum speed cannot be reached. Therefore, the optimal control contains only the first two phases. The third column corresponds to the case of large initial speeds and long-length roads. The vehicle starts with linearly decreasing acceleration, and then proceeds with no acceleration when the speed reaches the limit $v_{\max}$. Here, the optimal control contains only the last two phases. The last column corresponds to the case of large initial speeds and short-length roads. Therefore, the vehicle uses only linearly decreasing acceleration.

B. Fixed Terminal Time Optimal Control Problem

In this section, we consider the case where the optimal time t_p^* obtained in the free terminal time OCP (Problem 2) is within some red interval, that is, $t_p^* \in T_R$. In this case, the candidate optimal arrival time t_p^* in Problem 1 without (6) is either $\underline{t}_p$ or $\bar{t}_p$. Therefore, we can compare the performance obtained under either one of these two terminal times, and select the one with better performance to determine the optimal arrival time for Problem 1 without (6). In both cases, the travel time is now fixed, hence the only objective is to minimize the energy consumption. Thus, we have the following problem formulation.

Problem 3: Fixed terminal time OCP

$$\min_{u(t)} \int_{t_0}^{t_p} u^2(t) dt \tag{33}$$

$$\text{s. t. } (1), \; x(t_p) = l \tag{34}$$

$$t_p = \underline{t}_p \text{ or } \bar{t}_p \tag{35}$$

$$v_{\min} \leq v(t) \leq v_{\max} \tag{36}$$

$$u_{\min} \leq u(t) \leq u_{\max}. \tag{37}$$

Note that t_p is a fixed value here.

1) Arrival Time $t_p = \underline{t}_p$: In this case, it is clear that the vehicle must use less time than the one specified by t_p^* in Problem 2 and higher acceleration. Define a function

$$h(v_0) = \begin{cases} v_0 t_p + \frac{1}{2} u_{\max} t_p^2 - l, & \text{for } t_p \leq \frac{v_{\max} - v_0}{u_{\max}} \\ v_{\max} t_p - \frac{1}{2} \frac{(v_{\max} - v_0)^2}{u_{\max}} - l, & \text{for } t_p > \frac{v_{\max} - v_0}{u_{\max}}. \end{cases}$$

Observe that the terminal time $t_p = \underline{t}_p$ is possible if and only if $h(v_0) \geq 0$. The main result for this case is given in the following theorem.

Theorem 4: Consider the vehicle dynamics (1) with initial conditions $x(t_0) = 0$ and $v(t_0) = v_0$. Let $x^*(t)$, $v^*(t)$, $u^*(t)$ be an optimal solution to Problem 3 with $t_p = \underline{t}_p$. Then, the optimal control $u^*(t)$ satisfies

$$u^*(t) = \arg \min_{0 \le u(t) \le u_{\max}} u^2(t) + \frac{u^*(t_0)^2(t-\tau)u(t)}{v_0 - v^*(t_p) + (\tau - t_0)u^*(t_0)}$$

where τ is the first time on the optimal path when $v(\tau) = v_{\max}$ if $\tau < t_p$; $\tau = t_p$ otherwise.

Proof: Similar to the proof of Theorem 1, we will use the direct adjoining approach [30] to solve the fixed terminal time OCP. The Hamiltonian $H(v, u, \lambda)$ and Lagrangian $L(v, u, \lambda, \mu, \eta)$ are defined as $H(u, v, \lambda) = u^2 + \lambda_1 v + \lambda_2 u$, and $L(u, v, \lambda, \mu, \eta) = H + \mu(u - u_{\max}) + \eta_1(v_{\min} - v) + \eta_2(v - v_{\max})$, respectively, where $\lambda(t) = [\lambda_1(t)\ \lambda_2(t)]^T$ and $\eta(t) = [\eta_1(t)\ \eta_2(t)]^T$, and

$$\begin{aligned} &\mu(t) \ge 0, \quad \mu(t)[u^*(t) - u_{\max}] = 0 \\ &\eta_1(t) \ge 0, \quad \eta_2(t) \ge 0 \\ &\eta_1(t)[v_{\min} - v^*(t)] + \eta_2(t)[v^*(t) - v_{\max}] = 0. \end{aligned}$$

Since $\underline{t}_p \le t_p^*$, the optimal solution from the free terminal time optimal problem implies $u^*(t) \ge 0$ for all t. Therefore, the constraint $u(t) \ge u_{\min}$ is relaxed, and

$$u^*(t) = \arg \min_{0 \le u(t) \le u_{\max}} u^2 + \lambda_2 u \tag{38}$$

which implies that $u^*(t) = \min\{u_{\max}, -\lambda_2(t)/2\}$ and $\lambda_2(t) \le 0$. From the proof of Theorem 1, we know that $\mu(t)$ is a redundant variable, and λ_1 is a constant. Let us first assume that $l > v_{\min} t_p$. Note that the case of $l = v_{\min} t_p$ cannot occur when $t_p = \underline{t}_p$ (however, it may occur when $t_p = \bar{t}_p$ and this case will be discussed later). Again, we can prove the fact that $v(t) = v_{\min}$ happens only at $t = t_0$ but without using the transversality condition as we did in the free terminal time OCP. The property that $\lambda_2(t)$ has no discontinuities still holds. The costate $\lambda_2(t)$ satisfies

$$\dot{\lambda}_2(t) = -\lambda_1 + \eta_1(t) - \eta_2(t). \tag{39}$$

Similarly, we can show that $\eta_1(t) = 0$, and (39) reduces to $\dot{\lambda}_2(t) = -\lambda_1$ for $t \in [t_0, \tau)$ and $\lambda_2(\tau) = 0$. By solving the above differential equation, we get

$$\lambda_2(t) = -\lambda_1(t - \tau). \tag{40}$$

Again since the Hamiltonian is not an explicit function of time, by the condition $H(t_0) = H(t_p)$, we have

$$u^*(t_0)^2 + \lambda_1 v^*(t_0) - \lambda_1(t_0 - \tau)u^*(t_0) = \lambda_1 v^*(t_p) \tag{41}$$

where the fact that $\lambda_2(t_p) = u^*(t_p) = 0$ has been used. From (41), we can obtain

$$\lambda_1 = \frac{u^*(t_0)^2}{v^*(t_p) + (t_0 - \tau)u^*(t_p) - v^*(t_0)}. \tag{42}$$

For $t \in [\tau, t_p]$, we can just let $\eta_2(t) = -\lambda_1$. If $v^*(t_p) < v_{\max}$, then $\tau = t_p$ in (41). The proof is completed by substituting λ_1 in (42) into (40), and then λ_2 into (38). ■

Given the terminal time $\underline{t}_p$ and the road length l, the value of v_0 can be classified into one of the five cases as shown in Table II. Note that if Case i is infeasible for v_0 and the given parameters, we can treat J_i^u as infinity. The performance associated with each case in Table II as well as the detailed calculations are given in [29]. After obtaining the performance for each case with $t_p = \underline{t}_p$, we select the one with the smallest energy consumption, that is, $J_u^{\underline{t}_p} = \min\{J_1^u, \ldots, J_5^u\}$ with the corresponding optimal acceleration profile.

TABLE II
OPTIMAL SOLUTION CLASSIFICATION FOR PROBLEM 3 WITH $t_p = \underline{t}_p$

	Optimal Control	Performance
Case I	$u_0^* = u_{\max}$ until $v(t) = v_{\max}$ or t_p	J_1^u
Case II	$u^*(t_0) = u_{\max}$ and $v^*(t_p) = v_{\max}$	J_2^u
Case III	$u^*(t_0) = u_{\max}$ and $v^*(t_p) < v_{\max}$	J_3^u
Case IV	$u_0^* < u_{\max}$ and $v^*(t_p) = v_{\max}$	J_4^u
Case V	$u_0^* < u_{\max}$ and $v^*(t_p) < v_{\max}$	J_5^u

2) Arrival Time $t_p = \bar{t}_p$: In this case, the vehicle must use less acceleration than in the free terminal time case. Depending on the initial speed v_0, there are three cases to consider. First, if $l = v_0(\bar{t}_p - t_0)$, then the vehicle can cruise through the intersection with the constant speed v_0 without any acceleration (Case VI in Table III). The speed change value in this case is $J_6^u = 0$. If, on the other hand, $l > v_0(\bar{t}_p - t_0)$, then the problem can be solved using the result of the case $t_p = \underline{t}_p$ analyzed above. Finally, if $l < v_0(\bar{t}_p - t_0)$, then the vehicle must decelerate to reach the intersection while the traffic signal is in its green state. Therefore, the control input is only subject to the constraint $u_{\min} \le u(t) \le 0$. The main result in this case is given in Theorem 5.

Theorem 5: Consider the vehicle dynamics (1) with initial conditions $x(t_0) = 0$ and $v(t_0) = v_0$. Let $x^*(t)$, $v^*(t)$, $u^*(t)$ be an optimal solution to Problem 3 with $t_p = \bar{t}_p$. Then, the optimal solution $u^*(t)$ satisfies

$$u^*(t) = \arg \min_{u_{\min} \le u(t) \le 0} u^2(t) + \frac{u^*(t_0)^2(\tau - t)u(t)}{v^*(t_p) - v_0 - (\tau - t_0)u^*(t_0)}$$

where τ is the first time on the optimal path when $v(\tau) = v_{\min}$ if $\tau < t_p$; $\tau = t_p^*$ otherwise.

Proof: The Hamiltonian $H(u, v, \lambda)$ and the Lagrangian $L(u, v, \lambda, \mu, \eta)$ are defined as $H(u, v, \lambda) = u^2 + \lambda_1 v + \lambda_2 u$ and $L(u, v, \lambda, \mu, \eta) = H(u, v, \lambda) + \mu(u_{\min} - u) + \eta_1(v_{\min} - v) + \eta_2(v - v_{\max})$, respectively, where $\lambda(t) = [\lambda_1(t), \lambda_2(t)]^T$, $\eta(t) = [\eta_1(t), \eta_2(t)]^T$, $\mu(t) \ge 0$, $\mu(t)[u_{\min} - u^*(t)] = 0$, $\eta_1(t) \ge 0$, $\eta_2(t) \ge 0$ and $\eta_1(t)[v_{\min} - v^*(t)] + \eta_2(t)[v^*(t) - v_{\max}] = 0$. As before, we do not include the constraint $u(t) \le u_{\max}$ since we can establish that $u^*(t) \le 0$ similar to Lemma 2. According to Pontryagin's minimum principle, the optimal control $u^*(t)$ must satisfy $u^*(t) = \arg\min_{u_{\min} \le u(t) \le 0} H(v^*(t), u^*(t), \lambda(t))$ which allows us to express $u^*(t)$ in terms of the costate $\lambda(t)$, that is

$$u^*(t) = \max\left\{u_{\min}, -\frac{\lambda_2(t)}{2}\right\} \tag{43}$$

with $\lambda_2(t) \ge 0$. The Lagrange multiplier $\mu(t)$ is redundant as before. The costate λ_1 is a constant. The costate $\lambda_2(t)$ satisfies

TABLE III
OPTIMAL SOLUTION CLASSIFICATION FOR PROBLEM 3 WITH $t_p = \bar{t}_p$

	Optimal Control	Performance
Case VI	$u^*(t) = 0$ and $v^*(t) = v_0$	J_6^u
Case VII	$u^*(t_0) = u_{\min}$ and $v^*(t_p) = v_{\min}$	J_7^u
Case VIII	$u^*(t_0) = u_{\min}$ and $v^*(t_p) > v_{\min}$	J_8^u
Case IX	$u^*(t_0) < u_{\min}$ and $v^*(t_p) = v_{\min}$	J_9^u
Case X	$u^*(t_0) < u_{\min}$ and $v^*(t_p) > v_{\min}$	J_{10}^u

$\dot{\lambda}_2(t) = -\partial L^*/\partial v = -\lambda_1 + \eta_1(t) - \eta_2(t)$. First, it is easy to see that $v_0 \neq v_{\min}$. Let τ be the first time that $v(\tau) = v_{\min}$, then $u^*(t) = 0$ for $t \geq \tau$. Again, since the Hamiltonian is not an explicit function of time, by the condition $H^*(\tau^-) = H^*(\tau^+)$, we have

$$u^*(\tau^-)^2 + \lambda_2(\tau^-)u^*(\tau^-) = 0. \tag{44}$$

According to (43), we either have $u^*(\tau^-) = u_{\min}$ or $u^*(\tau^-) = -\lambda_2(\tau^-)/2$. When $u^*(\tau^-) = u_{\min}$, the above equality becomes $u_{\min}^2 + \lambda_2(\tau^-)u_{\min} = 0$, which contradicts the minimum principle (43); when $u^*(\tau^-) = -\lambda_2(\tau^-)/2$, (44) becomes $u^2(\tau^-) - 2u^2(\tau^-) = 0$. Therefore, only $\lambda_2(\tau^-) = u^*(\tau^-) = 0$ is possible, that is to say, λ_2 and u^* have no discontinuities at τ. At the terminal time t_p, the following costate boundary condition holds:

$$\lambda_2(t_p^-) = \gamma_1 \tfrac{\partial}{\partial v}[v_{\min} - v]|_{v=v^*(t_p)} + \gamma_2 \tfrac{\partial}{\partial v}[v - v_{\max}]|_{v=v^*(t_p)}$$

that is, $\lambda_2(t_p^-) = -\gamma_1 + \gamma_2$, $\gamma_1 \geq 0$, $\gamma_2 \geq 0$, and $\gamma_1[v_{\min} - v^*(t_p)] + \gamma_2[v^*(t_p) - v_{\max}] = 0$. At t_p, we know that $v^*(t_p) \neq v_{\max}$. Thus, $\gamma_2 = 0$. Likewise, it is easy to obtain $\gamma_1 = 0$. Therefore, we have $\lambda_2(t_p) = 0$. Since the Hamiltonian is not an explicit function of time, the condition $dH^*(t)/dt = 0$ implies that

$$[2u^*(t) + \lambda_2(t)]\dot{u}^*(t) + [\eta_1(t) - \eta_2(t)]u^*(t) = 0.$$

Since the first term is always zero as before, the above condition becomes $[\eta_1(t) - \eta_2(t)]u^*(t) = 0$. When $v_0 = v_{\max}$, we have $\eta_1(t_0) = 0$, that is, $\eta_2(t_0)u^*(t_0) = 0$. Recall that $\dot{\lambda}_2(t) = -\partial L^*/\partial v = -\lambda_1 + \eta_1(t) - \eta_2(t)$. Since $\lambda_1 > 0$, then $\lambda_2(t)$ must decrease. Therefore, $u^*(t_0) < 0$, and $\eta_2(t) = 0$ for all t. For $t \in [t_0, \tau)$, $\eta_1^*(t) = 0$. Therefore, $\dot{\lambda}_2(t) = -\lambda_1$ for $t \in [t_0, \tau)$. For $t \in [\tau, t_p)$, $\dot{\lambda}_2(t) = -\lambda_1 + \eta_1^*(t) = 0$. Solving the above differential equation, we obtain

$$\lambda_2(t) = \lambda_1(\tau - t) \tag{45}$$

for $t \in [t_0, \tau)$. By the condition $H(t_0) = H(t_p)$, we have

$$u^*(t_0)^2 + \lambda_1 v_0 + \lambda_1(\tau - t_0)u^*(t_0) = \lambda_1 v^*(t_p)$$

that is, $\lambda_1 = u^*(t_0)^2/[v^*(t_p) - v_0 - (\tau - t_0)u^*(t_0)]$. The proof is completed by substituting λ_1 into (45) and then λ_2 into (43). ■

The classification of all possible solutions with $t_p = \bar{t}_p$ is shown in Table III. The performance associated with each case in this table as well as the detailed calculations are given in [29]. After obtaining the performance J_u from J_6^u through J_{10}^u, we can select $J_u^{\bar{t}_p} = \min\{J_6^u, \ldots, J_{10}^u\}$, where J_i^u can be treated as infinity if Case i is infeasible. Finally, we can compare the two performances obtained, that is

$$J^{\underline{t}_p} = \rho_t(\underline{t}_p - t_0) + \rho_u J_u^{\underline{t}_p}, \quad J^{\bar{t}_p} = \rho_t(\bar{t}_p - t_0) + \rho_u J_u^{\bar{t}_p}$$

and determine the optimal performance to be the one with a smaller value. Therefore, Algorithm 1 solves Problem 1 without the constraint (6) optimally.

Algorithm 1: ECO-AND Algorithm

Input: ρ_t, ρ_u, l, v_0, $v_{\min}$, $v_{\max}$, $u_{\min}$, $u_{\max}$, T_G, t_0
Output: t_p^*, $v^*(t)$, $u^*(t)$
Initialization: Solve Problem 2 using Theorem 1 to obtain t_p, $v(t)$, $u(t)$
if $t_p \in T_G$ **then**
  $t_p^* \leftarrow t_p$, $v^*(t) \leftarrow v(t)$, $u^*(t) \leftarrow u(t)$
  stop
else
  Obtain $\underline{t}_p$ and $\bar{t}_p$
  Solve Problem 3 with $t_p = \underline{t}_p$ using Theorem 4 to obtain $J^{\underline{t}_p}$, $v_1(t)$, $u_1(t)$
  switch $s = l - v_0(\bar{t}_p - t_0)$ **do**
    case $s = 0$ **do**
      $J^{\bar{t}_p} = \bar{t}_p$, $v_2(t) = v_0$, $u_2(t) = 0$
    case $s > 0$ **do**
      Solve Problem 3 with $t_p = \bar{t}_p$ using Theorem 4 to obtain $J^{\bar{t}_p}$, $v_2(t)$, $u_2(t)$
    case $s < 0$ **do**
      Solve Problem 3 with $t_p = \bar{t}_p$ using Theorem 5 to obtain $J^{\bar{t}_p}$, $v_2(t)$, $u_2(t)$
  if $J^{\bar{t}_p} \geq J^{\underline{t}_p}$ **then**
    $t_p^* = \underline{t}_p$, $v^*(t) \leftarrow v_1(t)$, $u^*(t) \leftarrow u_1(t)$
  else
    $t_p^* = \bar{t}_p$, $v^*(t) \leftarrow v_2(t)$, $u^*(t) \leftarrow u_2(t)$
  stop

In the following, we will show how the algorithm can be extended to provide a suboptimal solution to Problem 1 when constraint (6) is included.

IV. EXTENSION TO CASES WITH INTERFERING TRAFFIC

Recall that in all results given in Section III the safe distance constraint (6) was relaxed. Now, we will show how to adjust the optimal control solution without the consideration of (6) to include the safety constraint based on the assumption that vehicles can exchange information via vehicle-to-vehicle (V2V) communication. Additional assumptions include the following.

1) On the road, the future speed and acceleration profiles of the preceding vehicle can be transmitted to the autonomous vehicles.

2) At the intersection, the queue information and the stopped vehicle lengths are available to the following vehicles.

The movement of the autonomous vehicle under the optimal controller without considering (6) may be affected by other road users. There are three such cases in what follows.

1) The first case is that the preceding vehicle will cross the intersection at some time $t \in T_G$ while the autonomous vehicle will not cross the intersection at the same green interval as the preceding vehicle because it is slowed down while enforcing (6). The optimal arrival time for the autonomous vehicle is the beginning of the next green interval, and the autonomous vehicle becomes the leading vehicle on the road. Then, the optimal acceleration profile can be obtained by using the fixed terminal optimal control algorithm in Section III-B. If the safety constraint is violated, the autonomous vehicle switches to a car-following mode.
2) The second case is that both the preceding vehicle and the autonomous vehicle will cross the intersection at the same green light interval. In this case, we can create a time gap, for example, the two-second rule, between the autonomous vehicle and the preceding vehicle at the intersection. The optimal acceleration profile will be obtained by solving the fixed terminal time OCP in Section III-B. If the safety constraint (6) is violated, the autonomous vehicle switches to a car-following mode.
3) The third case is that the preceding vehicle is forced to stop before the intersection due to the presence of queued vehicles waiting for the traffic signal turning green. In this case, the autonomous vehicle will cross the intersection when the traffic signal turns green after the preceding vehicle with a certain time gap σ, for example, the two-second rule. The optimal acceleration profile will be obtained by solving the fixed terminal time OCP in Section III-B. If the safety constraint is violated, the autonomous vehicle switches to a car-following mode.

V. Numerical Examples

We have simulated the system defined by the vehicle dynamics (1). Associated parameters in the OCP are given as follows. The minimum and maximum speeds are 2.78 and 22.22 m/s. The maximum acceleration and deceleration are set to 2.5 and -2.9 m/s^2, respectively. Fig. 1 shows the travel time and the energy consumption when we vary the parameter ρ from 0 to 1. The initial speed is chosen as $v_0 = 18.6182$ and the length of the road 200 m. By exploring the tradeoff curve, one may select an appropriate weight parameter ρ depending on a particular application of interest. For instance, if energy efficiency is a major concern, Fig. 1 suggests not to select a large value for ρ since the energy consumption grows rapidly as ρ approaches 1. On the other hand, a small ρ is unlikely a good option, since we can see that energy consumption does not significantly increase with ρ increasing as long as $\rho < 0.7$ (approximately). In fact, when ρ increases from 0 to 0.7,

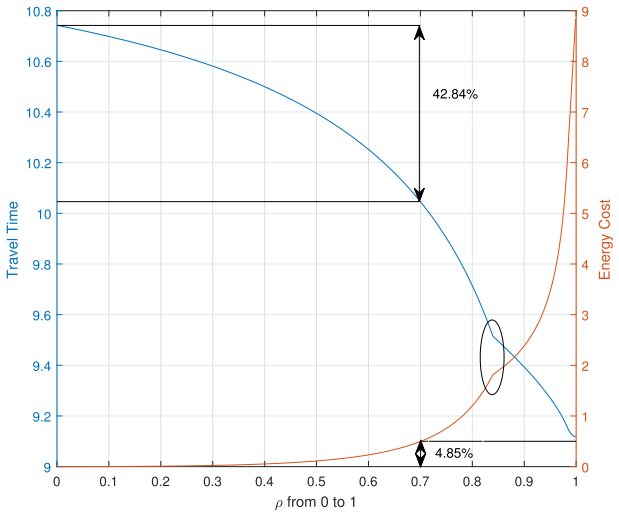

Fig. 1. Trade-off between travel time and energy consumption.

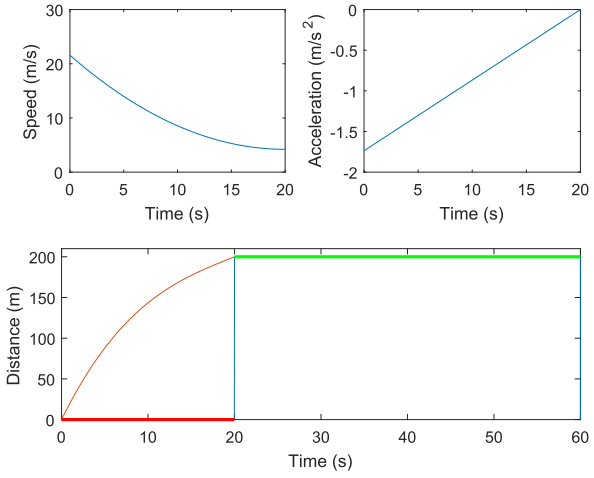

Fig. 2. Case X in Table III with $v_0 = 21.5791$.

the travel time is significantly reduced by 42.84% whereas the energy consumption increases by only 4.85%. It is noteworthy that both curves show different trends around the circled area shown in Fig. 1: this is mainly because the vehicle has reached the speed limit when the parameter ρ is large. When the parameter ρ is further increased close to 1, the maximum acceleration is included in the optimal acceleration profile, and the energy cost surges.

In the following, the weights in (2) are set using $\rho = 0.9549$, that is, $\rho_t = 0.0133$, and $\rho_u = 9.2798 \times 10^{-4}$. In this case, the values $1 - u_{\max}^2 \rho_u / \rho_t = 0.5630$ and $(v_m + v_M)/(2v_M) = 0.5626$ are almost the same. Thus, if we randomly generate the initial speed v_0 from a uniform distribution on the interval $[v_{\min}, v_{\max}]$, different initial speeds fall roughly equally into the two different cases in the first row in Table I. The total cycle time for the traffic light is 60 s with different patterns. We first test the optimal controller on a road of length 200 m. Fig. 2 exhibits a traffic light pattern, where the phase of the traffic signal in the first 20 s is red. Due to a relatively large initial speed, the vehicle has to decelerate to cross the intersection when the traffic light is green.

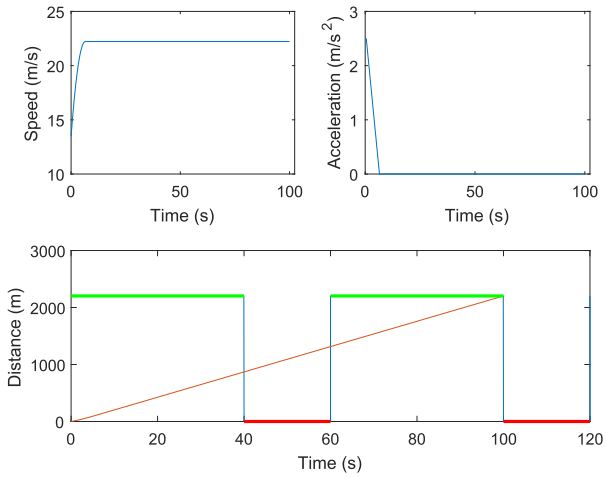

Fig. 3. Case II in Table II with $v_0 = 13.4875$.

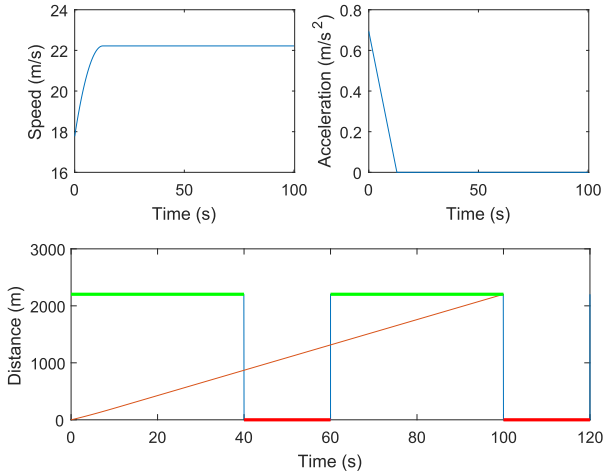

Fig. 4. Case IV in Table II with $v_0 = 17.7745$.

In the following, we test the optimal controller on a road of length 2203 m. Due to this length, the optimal arrival time usually does not fall within the first green light cycle, and sometimes it is impossible for the vehicle to arrive at the intersection within the current cycle. For the case in Fig. 3, the optimal arrival time calculated from the free terminal time OCP is 102.3476 s. Unfortunately, this arrival time belongs to a red interval. Therefore, full acceleration is used to reach the speed limit and cross the intersection at 100 s when the phase of the traffic signal is green. Fig. 4 shows the case when the vehicle has a relatively fast initial speed compared to Fig. 3. Therefore, the vehicle does not start with full acceleration to reach the speed limit and catch the green phase at 100 s. For the last case in Fig. 5, the initial speed is very large. However, it is impossible for the vehicle to cross the intersection by the end of the second green cycle at 90 s due to the speed limit constraint. The best option is to decelerate the vehicle to cross the intersection at 120 s when the traffic light just turns green.

A. Effect of Interfering Traffic

Here, we consider traffic conditions where a vehicle enters a road at time 3.1982 s and there is a preceding vehicle in front of it. The driving behavior of both the preceding vehicle and the following vehicle are generated by the data recorded from the traffic system simulator VISSIM. The initial speed of the following vehicle is 15.0086 m/s and the distance of the following vehicle to the traffic signal head is 245.1286 m at time 3.1982 s. The current phase of the traffic signal is red, and the time to green is 14.8916 s. We replace the human-driven following vehicle by an autonomous vehicle and apply the ECO-AND algorithm to the autonomous vehicle without considering the preceding vehicle. The trajectory of the autonomous vehicle will be obstructed by the preceding vehicle. In this case, we assume that the autonomous vehicle is able to obtain the speed profile of the preceding vehicle based on V2V communication. We set the intersection crossing time of the autonomous vehicle the same as the human-driven following vehicle at $t_p = 22.7753$ s. A certain safety gap between the autonomous vehicle and the preceding vehicle is guaranteed as shown in Fig. 6, and the safety gap is larger than that between the preceding vehicle and the human-driven following vehicle. Fig. 6 also shows the acceleration profile and speed profile of the preceding vehicle, the following vehicle, and the autonomous vehicle when it replaces the following vehicle, respectively. As seen from the figures, the autonomous vehicle chooses to decelerate from the beginning which is determined by comparing the optimal performance between acceleration (Theorem 4) and deceleration (Theorem 5). From a driving comfort point of view, there is less variation of the speed of the autonomous vehicle even though the interfering traffic is considered. By using the fuel consumption model proposed in [18]

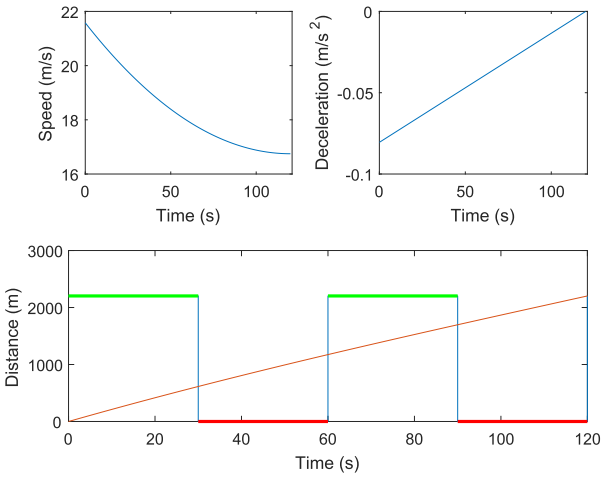

Fig. 5. Case X in Table III with $v_0 = 21.5791$.

$$\dot{m}_f = \begin{cases} \alpha_0 + \alpha_1 v + \alpha_2 v^2 + \alpha_3 v^3 \\ \quad +(\beta_0 + \beta_1 v + \beta_2 v^2)u, & u \geq 0 \\ \alpha_0, & u < 0 \end{cases} \tag{46}$$

where $\dot{m}_f$ is the fuel consumption rate, and the numerical values of model parameters α_i and β_i are given in [18], the human-driven following vehicle consumes 6.8807-mL fuel. However, the autonomous vehicle uses only 3.0717-mL

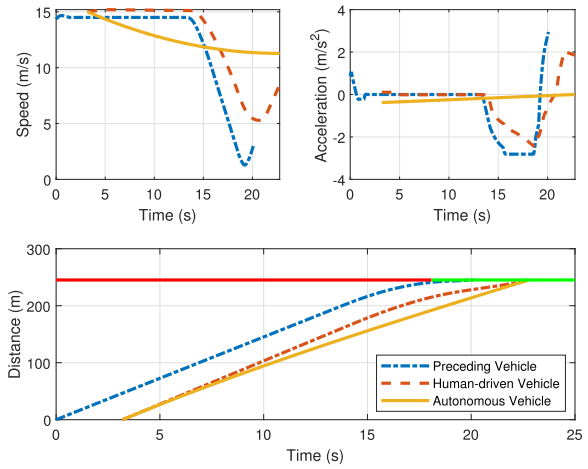

Fig. 6. Optimal control of the autonomous vehicle with interfering traffic.

fuel, which is less than half of the fuel consumed by the human-driven following vehicle.

B. Intersection Performance Evaluation

In the objective function (2), we use J^u as a measure of speed variations and the speed profile is designed based on the vehicle dynamic model (1). Such a simplification enables us to apply the proposed algorithm in real-time. In order to show the effectiveness of the proposed method, we evaluate the intersection performance in VISSIM for different vehicle compositions. In addition, to strengthen the applicability of the proposed ECO-AND algorithm, in contrast to the simulation results in Section V-A there is no V2V communication in the simulation setup and autonomous vehicles simply switch to the car-following mode when safety constraints are violated. An identical setup is used to evaluate three different cases: 1) 100% autonomous vehicles; 2) 100% conventional vehicles; and 3) 50% autonomous vehicles and 50% conventional vehicles (non-free flow case). A road about 330 m with two lanes (left-turn lane and straight ahead lane) is considered. The traffic volume is set to be 600 vehicles per hour for each case. The data about 600 vehicles of each case are collected during an hour simulation time. All vehicles use the Wiedemann 74 car-following model and the free lane selection rule is used for modeling the lane changing behavior in VISSIM. The autonomous vehicles receive the signal phase and time information within a distance of 250 m to the traffic signal head. The signal cycle time is 60 s (9-s green, 4-s amber, 47-s red). The calculated optimal speed profiles are used as desired speed profiles for autonomous vehicles. The actual speed of an autonomous vehicle may not be the same as the desired speed when the safety constraint is violated. In this case, the autonomous vehicles' driving behavior switches to the Wiedemann 74 car-following model. Two performance indices are evaluated: fuel consumption and vehicle delay, which is obtained by subtracting the theoretical travel time from the actual travel time. The theoretical travel time is the travel time which could be achieved if there were no other vehicles and/or signal controls. For case 1), the total fuel consumption for about 600 vehicles in an hour is 10.583 gallons and the delay for all autonomous vehicles is 57.98 min. For case 2), the fuel consumption is about 21.957 gallons and the delay for all conventional vehicles is 225.26 min. For case 3), the total fuel consumption is 10.876 gallons, the delay for all vehicles 63.78 min. Compared with conventional vehicles, the improvements are 51.80%, and 74.26% for the fuel consumption, and vehicle delay, respectively. For the case of 50% penetration rate, the improvements are 50.46% and 71.68% for the fuel consumption and vehicle delay, respectively, thus showing the positive impact of autonomous vehicles on conventional vehicles.

VI. Conclusion

This article derives an optimal acceleration/deceleration profile for autonomous vehicles approaching an intersection based on the traffic signal information obtained from an intelligent infrastructure via V2I communication. The solution for the above problem has the key feature of avoiding idling at an intersection when the phase of the traffic signal is red. Comparing with similar problems solved by numerical calculations, we provide a real-time analytical solution. The proposed algorithm offers better efficiency in terms of travel time and energy consumption, which has been verified through extensive simulations. The simulation results show that the eco-driving algorithm achieves substantial performance improvement compared with vehicles with human driver behavior. In extending this work, there is a need to consider a practical scenario where multiple autonomous vehicles cooperate to cross a signalized intersection.

References

[1] D. Schrank, B. Eisele, T. Lomax, and J. Bak, "2015 urban mobility scorecard," Texas A&M Transp. Inst. INRIX, Kirkland, WA, USA, Tech. Rep., 2015.

[2] S. Lefevre, A. Carvalho, and F. Borrelli, "A learning-based framework for velocity control in autonomous driving," *IEEE Trans. Autom. Sci. Eng.*, vol. 13, no. 1, pp. 32–42, Jan. 2016.

[3] L. Li, D. Wen, and D. Yao, "A survey of traffic control with vehicular communications," *IEEE Trans. Intell. Transp. Syst.*, vol. 15, no. 1, pp. 425–432, Feb. 2014.

[4] E. Hellström, J. Åslund, and L. Nielsen, "Design of an efficient algorithm for fuel-optimal look-ahead control," *Control Eng. Pract.*, vol. 18, no. 11, pp. 1318–1327, Nov. 2010.

[5] S. E. Li, H. Peng, K. Li, and J. Wang, "Minimum fuel control strategy in automated car-following scenarios," *IEEE Trans. Veh. Technol.*, vol. 61, no. 3, pp. 998–1007, Mar. 2012.

[6] J. L. Fleck, C. G. Cassandras, and Y. Geng, "Adaptive quasi-dynamic traffic light control," *IEEE Trans. Control Syst. Technol.*, vol. 24, no. 3, pp. 830–842, May 2016.

[7] V. Milanes, J. Perez, E. Onieva, and C. Gonzalez, "Controller for urban intersections based on wireless communications and fuzzy logic," *IEEE Trans. Intell. Transp. Syst.*, vol. 11, no. 1, pp. 243–248, Mar. 2010.

[8] S. Huang, A. W. Sadek, and Y. Zhao, "Assessing the mobility and environmental benefits of reservation-based intelligent intersections using an integrated simulator," *IEEE Trans. Intell. Transp. Syst.*, vol. 13, no. 3, pp. 1201–1214, Sep. 2012.

[9] K.-D. Kim and P. R. Kumar, "An MPC-based approach to provable system-wide safety and liveness of autonomous ground traffic," *IEEE Trans. Autom. Control*, vol. 59, no. 12, pp. 3341–3356, Dec. 2014.

[10] A. A. Malikopoulos, C. G. Cassandras, and Y. J. Zhang, "A decentralized energy-optimal control framework for connected automated vehicles at signal-free intersections," *Automatica*, vol. 93, pp. 244–256, Jul. 2018.

[11] J. Rios-Torres and A. A. Malikopoulos, "A survey on the coordination of connected and automated vehicles at intersections and merging at highway on-ramps," *IEEE Trans. Intell. Transp. Syst.*, vol. 18, no. 5, pp. 1066–1077, May 2017.
[12] F. Borrelli, A. Bemporad, and M. Morari, *Predictive Control for Linear and Hybrid Systems*. Cambridge, U.K.: Cambridge Univ. Press, 2017.
[13] W. Xiao, C. G. Cassandras, and C. Belta, "Decentralized merging control in traffic networks with noisy vehicle dynamics: A joint optimal control and barrier function approach," in *Proc. IEEE Intell. Transp. Syst. Conf. (ITSC)*, Oct. 2019, pp. 3162–3167.
[14] X. Meng and C. G. Cassandras, "Optimal control of autonomous vehicles for non-stop signalized intersection crossing," in *Proc. IEEE Conf. Decis. Control (CDC)*, Dec. 2018, pp. 6988–6993.
[15] P. Hao, G. Wu, K. Boriboonsomsin, and M. J. Barth, "Eco-approach and departure (EAD) application for actuated signals in real-world traffic," *IEEE Trans. Intell. Transp. Syst.*, vol. 20, no. 1, pp. 30–40, Jan. 2019.
[16] B. Asadi and A. Vahidi, "Predictive cruise control: Utilizing upcoming traffic signal information for improving fuel economy and reducing trip time," *IEEE Trans. Control Syst. Technol.*, vol. 19, no. 3, pp. 707–714, May 2011.
[17] S. E. Li, S. Xu, X. Huang, B. Cheng, and H. Peng, "Eco-departure of connected vehicles with V2X communication at signalized intersections," *IEEE Trans. Veh. Technol.*, vol. 64, no. 12, pp. 5439–5449, Dec. 2015.
[18] N. Wan, A. Vahidi, and A. Luckow, "Optimal speed advisory for connected vehicles in arterial roads and the impact on mixed traffic," *Transp. Res. C, Emerg. Technol.*, vol. 69, pp. 548–563, Aug. 2016.
[19] O. D. Altan, G. Wu, M. J. Barth, K. Boriboonsomsin, and J. A. Stark, "GlidePath: Eco-friendly automated approach and departure at signalized intersections," *IEEE Trans. Intell. Vehicles*, vol. 2, no. 4, pp. 266–277, Dec. 2017.
[20] C. Sun, X. Shen, and S. Moura, "Robust optimal ECO-driving control with uncertain traffic signal timing," in *Proc. Annu. Amer. Control Conf. (ACC)*, Jun. 2018, pp. 5548–5553.
[21] G. Mahler and A. Vahidi, "An optimal velocity-planning scheme for vehicle energy efficiency through probabilistic prediction of traffic-signal timing," *IEEE Trans. Intell. Transp. Syst.*, vol. 15, no. 6, pp. 2516–2523, Dec. 2014.
[22] G. De Nunzio, C. C. de Wit, P. Moulin, and D. Di Domenico, "Eco-driving in urban traffic networks using traffic signals information," *Int. J. Robust Nonlinear Control*, vol. 26, no. 6, pp. 1307–1324, Apr. 2016.
[23] Q. Lin *et al.*, "Minimize the fuel consumption of connected vehicles between two red-signalized intersections in urban traffic," *IEEE Trans. Veh. Technol.*, vol. 67, no. 10, pp. 9060–9072, Oct. 2018.
[24] X. Meng and C. G. Cassandras, "Trajectory optimization of autonomous agents with spatio-temporal constraints," *IEEE Trans. Control Netw. Syst.*, vol. 7, no. 3, pp. 1571–1581, Sep. 2020.
[25] M. A. S. Kamal, M. Mukai, J. Murata, and T. Kawabe, "Model predictive control of vehicles on urban roads for improved fuel economy," *IEEE Trans. Control Syst. Technol.*, vol. 21, no. 3, pp. 831–841, May 2013.
[26] A. Ferrara, S. Sacone, and S. Siri, *Freeway Traffic Modelling and Control* (Advances in Industrial Control). Cham, Switzerland: Springer, 2018.
[27] A. A. Malikopoulos and J. P. Aguilar, "An optimization framework for driver feedback systems," *IEEE Trans. Intell. Transp. Syst.*, vol. 14, no. 2, pp. 955–964, Jun. 2013.
[28] S. Xu, S. E. Li, X. Zhang, B. Cheng, and H. Peng, "Fuel-optimal cruising strategy for road vehicles with step-gear mechanical transmission," *IEEE Trans. Intell. Transp. Syst.*, vol. 16, no. 6, pp. 3496–3507, Dec. 2015.
[29] X. Meng and C. G. Cassandras, "Optimal control of autonomous vehicles approaching a traffic light," 2018, *arXiv:1802.09600*. [Online]. Available: http://arxiv.org/abs/1802.09600
[30] R. F. Hartl, S. P. Sethi, and R. G. Vickson, "A survey of the maximum principles for optimal control problems with state constraints," *SIAM Rev.*, vol. 37, no. 2, pp. 181–218, Jun. 1995.
[31] A. E. Bryson and Y. C. Ho, *Applied Optimal Control: Optimization, Estimation and Control*. Boca Raton, FL, USA: CRC Press, 1975.

Xiangyu Meng received the Ph.D. degree in control systems from the University of Alberta, Edmonton, AB, Canada, in 2014.

He is currently an Assistant Professor with the Division of Electrical and Computer Engineering, Louisiana State University, Baton Rouge, LA, USA. He was a Research Associate with the Department of Mechanical Engineering, The University of Hong Kong, Hong Kong, from June 2007 to July 2007 and from November 2007 to January 2008. He was a Research Award Recipient in the Department of Electrical and Computer Engineering, University of Alberta, from February 2009 to August 2010. From December 2014 to December 2016, he was with the School of Electrical and Electronic Engineering, Nanyang Technological University, Singapore, as a Research Fellow. He was a Post-Doctoral Associate with the Division of Systems Engineering, Boston University, Brookline, MA, USA, from January 2017 to December 2018. His research interests include smart cities, connected and autonomous vehicles, and cyber-physical systems.

Christos G. Cassandras (Life Fellow, IEEE) received the B.S. degree from Yale University, New Haven, CT, USA, the M.S.E.E. degree from Stanford University, Stanford, CA, USA, and the M.S. and Ph.D. degrees from Harvard University, Cambridge, MA, USA.

He is a Distinguished Professor of Engineering at Boston University, Brookline, MA, USA, the Head of the Division of Systems Engineering, and a Professor of Electrical and Computer Engineering. From 1982 to 1984, he was with ITP Boston, Inc., Cambridge, where he was involved in the design of automated manufacturing systems. From 1984 to 1996, he was a Faculty Member with the Department of Electrical and Computer Engineering, University of Massachusetts Amherst, Amherst, MA, USA. He has authored over 450 refereed papers and six books in these areas. He specializes in the areas of discrete event and hybrid systems, cooperative control, stochastic optimization, and computer simulation, with applications to computer and sensor networks, manufacturing systems, and transportation systems.

Dr. Cassandras is a fellow of the International Federation of Automatic Control (IFAC). He was the President of the IEEE Control Systems Society in 2012. He is also a member of Phi Beta Kappa and Tau Beta Pi. He was a recipient of several awards, including the 2011 IEEE Control Systems Technology Award, the 2006 Distinguished Member Award of the IEEE Control Systems Society, the 1999 Harold Chestnut Prize (IFAC Best Control Engineering Textbook), a 2011 Prize and a 2014 Prize for the IBM/IEEE Smarter Planet Challenge Competition, the 2014 Engineering Distinguished Scholar Award at Boston University, several honorary professorships, the 1991 Lilly Fellowship, and the 2012 Kern Fellowship. He was the Editor-in-Chief of the IEEE TRANSACTIONS ON AUTOMATIC CONTROL from 1998 to 2009. He serves on several editorial boards and has been a guest editor for various journals.